

Silicene: from monolayer to multilayer — A concise review*

Li Hui(李 晖)[†], Fu Hui-Xia(付会霞), and Meng Sheng(孟 胜)

Beijing National Laboratory for Condensed Matter Physics and Institute of Physics, Chinese Academy of Sciences, Beijing 100190, China

(Received 13 March 2015; revised manuscript received 20 May 2015; published online 20 July 2015)

Silicene, a newly isolated silicon allotrope with a two-dimensional (2D) honeycomb lattice structure, is predicted to have electronic properties similar to those of graphene, including the existence of signature Dirac fermions. Furthermore, the strong spin-orbit interaction of Si atoms potentially makes silicene an experimentally accessible 2D topological insulator. Since 2012, silicene films have been experimentally synthesized on Ag (111) and other substrates, motivating a burst of research on silicene. We and collaborators have employed STM investigations and first principles calculations to intensively study the structure and electronic properties of silicene films on Ag (111), including monolayer, bilayer, and multilayer silicenes, as well as hydrogenation of silicene.

Keywords: silicene, STM, STS, first principles calculation

PACS: 61.46.-w, 68.37.Ef, 73.22.-f, 81.05.Zx

DOI: 10.1088/1674-1056/24/8/086102

1. Introduction

Graphene, a slice of sp^2 -bonded carbon film from bulk graphite, has brought a storm of discoveries about two-dimensional (2D) materials in the last decade in the fields of physics, chemistry, and material science, due to graphene's unique Dirac-type electronic structure and outstanding properties such as high thermal and electrical conductivity, mechanical stability, and inert chemical reactivity.^[1] Beyond graphene, people are searching for other elemental 2D materials. One attractive material is silicene, the one-atom-thick silicon film with a honeycomb lattice, first predicted based on first principles calculation.^[2] Free-standing silicene adopts a low-buckled 2D structure with a buckling distance of ~ 0.4 Å. As silicene is the silicon analog of graphene, many properties of graphene have been predicted also to exist for silicene, including the signature Dirac fermions. Furthermore, the predicted relativistic Dirac fermions, which are due to spin orbital coupling (SOC) being stronger in silicon than in carbon, would make single-layer silicene (SLS) a potential 2D topological insulator, expected to yield an observable spin quantum-Hall effect.^[3,4] Multilayer silicene (MLS) films also demonstrate interesting electronic properties, such as chiral superconducting behavior,^[5] valley-polarized quantum Hall effect,^[6] and electronic structure that is dramatically tunable by varying stacking modes.^[7,8] It is also commonly proposed that silicene is more compatible with silicon-based industry.

Within the past three years, great progress has also been made in the field of experimental synthesis of silicene.^[9–29]

Unlike graphene, which can be exfoliated from van der Waals (vdW)-packed graphite, sp^2 -hybridized silicon does not exist in nature. Thus, silicene can be achieved only by stabilizing interfacial interaction with a substrate. So far, although growth of monolayer silicon film has been reported on several substrates such as ZrB_2 ,^[11] Ir (111),^[12] and Ag (110),^[23] more than 90% of the research reports on silicene focus on silicene epitaxially grown on Ag (111) surface.^[9,10,13–22] Both SLS and MLS have been grown on Ag (111) surface using molecular beam epitaxy (MBE) and intensively studied by scanning tunneling microscopy (STM) and angle-resolved photoemission spectroscopy (ARPES), combined with first principles calculations. However, the atomic structure of silicene on Ag (111) is still under heavy debate, because it has been found that SLS can assume numerous metastable structures on Ag (111), depending on growth temperature and dynamics, such as 3×3 , $2\sqrt{3}\times 2\sqrt{3}$, and $\sqrt{3}\times\sqrt{3}$ surface reconstructions with respect to the Si (111)- 1×1 lattice.^[10] Among these reconstructions, the $\sqrt{3}\times\sqrt{3}$ -R30° structure is believed to be closest to isolated silicene, since it exhibits reversible dynamical phase transitions at low temperatures and weaker bonding to silver substrate^[18,19,21] than other metastable structures. Quasiparticle interference (QPI) pattern analysis^[18] and ARPES measurement^[14] both reveal linear band dispersions in such a $\sqrt{3}\times\sqrt{3}$ structure. Recently, MLS structures have also drawn much attention.^[22–29] It has been found that MLS can form the unique $\sqrt{3}\times\sqrt{3}$ structure only on Ag (111), and adopts a diamond-like stacking mode.^[22,28] It is interesting that such diamond-like silicon structures still exhibit a linear

*Project supported by the National Natural Science Foundation of China (Grant Nos. 11334011, 11222431, and 11322431), the National Basic Research Program of China (Grant Nos. 2012CB921403, 2013CBA01600, and 2012CB921703), the “Strategic Priority Research Program” of the Chinese Academy of Sciences, and the Hundred Talents Program of Institute of Physics, Chinese Academy of Sciences.

[†]Corresponding author. E-mail: huili8@iphy.ac.cn

dispersion surface state, which is observed in both ARPES^[24] and QPI from STS.^[22] Furthermore, it is remarkable that MLS is found to show great stability in air, while in contrast, SLS is easily oxidized by oxygen and water.^[26] The preserved Dirac fermions and robustness in air indicate MLS has great potential in practical applications of silicene.

On the other hand, silicon atoms in silicene have partial sp^3 -hybridization, displaying much higher reactivity than purely sp^2 -hybridized carbon atoms in graphene. Thus, silicene is easier to dope with other atoms, which can dramatically modify the electronic properties.^[30–34] For example, first principles calculations predict that hydrogenation can open a large band gap (~ 3 eV) for silicone,^[30] and that halide-doped silicene can be a large-gap 2D topological insulator. Recent experiment has confirmed silicene is much easier to be hydrogenated than graphene.^[34] The doped silicene also launches a new field for making electronic devices based on silicene.

In this review, we will introduce previous theoretical predictions of the structure of silicene (Section 2), the recent development of SLS and MLS grown on Ag (111) surface and other substrates (Section 3), as well as some of the newest results on hydrogenated silicene (Section 4).

2. The properties of free-standing silicene

2.1. Structure of monolayer silicene

The properties of free-standing monolayer silicene were first predicted using first principles calculations in the framework of density functional theory (DFT) by Ciraci *et al.* in 2009,^[2] and even before that, monolayer silicon layer had already been theoretically studied.^[35] As shown in the potential energy surface (PES) plot as a function of the lattice constant (Fig. 1(c)), three local energy minima can be obtained for monolayer silicon honeycomb sheet, the high-buckled (HB), the low-buckled (LB), as well as the planar (PL) structures. The HB structure is closer to a bilayer silicon film. According to the phonon calculation and finite temperature molecular dynamics (MD) simulation, the PL structure can spontaneously transform to the LB structure, and the LB silicene is thermodynamically stable. Thus, the LB structure of silicon, now called silicene, can theoretically exist. As shown in Figs. 1(a) and 1(b), the optimized lattice constant of free-standing silicene is 0.387 nm, and the buckling depth is ~ 0.4 Å based on our DFT calculations. The band structure (Fig. 1(d)) demonstrates a linear dispersive Dirac cone at the K points in the first Brillouin zone of silicene.

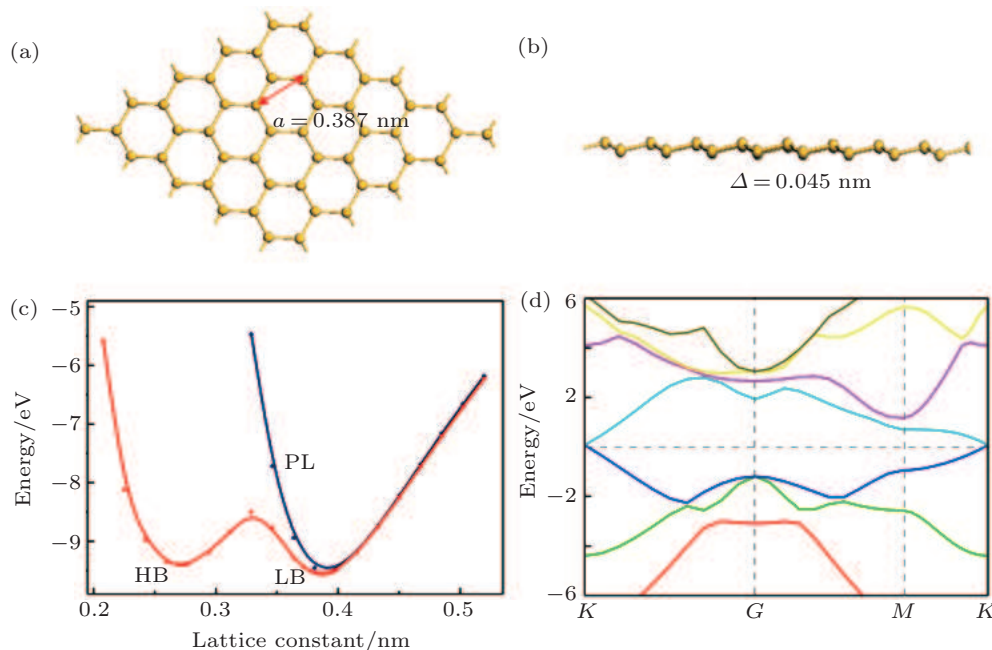


Fig. 1. (a) The side and (b) top view of free-standing low-buckled silicene obtained from DFT calculation. (c) The potential energy surface (PES) of silicene versus lattice constant. (d) The calculated band structure of low-buckled silicene.

2.2. Structure of bilayer silicene

The details of isolated SLS are now well known, but despite great efforts in the last decade to explore the atomic and electronic structures of bilayer silicon (BLS) films, these

structures remain unclear.^[36] For example, the widely used BLS model is the AB (Bernal) stacked model; however, using first principles calculation, Zeng *et al.* predicted a planar covalent-bonded silicon bilayer with AA-stacking mode,^[8] Morishita *et al.* reported a re-DL-Si morphology from re-

construction of two-layer Si (111) surface,^[37] and Xiang *et al.* predicted an Si-Cmme quasi-bilayer structure, using global optimization.^[38] It is well known that both interlayer interaction and stacking order play key roles in determining the properties of multilayer silicene. Unlike van der Waals stacking in bilayer graphene, whose global minimum is AB-stacked, BLS has been proposed to have various morphologies due to complicated interlayer covalent bonds.^[39]

We employed a method similar to that used for studying SLS to search for stable and functional BLS based on DFT calculations.^[7] The PBE functional^[40] was employed for structural research of BLS, and the HSE functional^[41] was used for electronic structure calculation. The projector augmented wave (PAW) pseudopotentials combined with plane-wave basis set (energy cutoff at 250 eV) were used with the Vienna *ab initio* Simulation Package (VASP).^[42] By scanning the PES of bilayer silicon sheets related to the lattice constant and starting with AA and AB stacking modes (Fig. 2(e)), several metastable configurations of BLS have been found, which are named by the combination of stacking mode and the order of cohesive energies. Among these minima, the most stable BLS morphology, 1AA, is the previously predicted planar AA-stacking BLS (Fig. 2(a)). The most stable AB-stacking BLS, 1AB is the widely used BLS model (Fig. 2(b)). We also found a vdW-packed BLS isomer, 2AA (Fig. 2(c)), which has energy comparable to that of 1AB. According to MD simulation, we further found a new stable structure of BLS, in which the two silicene layers are slightly staggered with respect to each other, and we named the structure slide-2AA.

Although the cohesive energies of these BLS morphologies are not much different, they demonstrate a variety of distinct electronic properties. The calculations show that the 2AA isomer has a semimetal electronic structure, in which the energy gap is 0, but the density of state (DOS) is also 0 at the Fermi level. The stable structure of BLS in our calculations, slide-2AA, is a semiconductor with a significant band gap of 1.16 eV (HSE level), while all the other morphologies of BLS are metallic or semimetallic. It is further found that the transition barriers between 2AA, 1AB, and slide-2AA (~ 29 meV/Si) are very close to the interlayer sliding barrier of graphite,^[43] indicating we can easily change the stacking mode of BLS, thereby tuning their electronic properties. The unique relationship of structure and electronic properties in BLS has profound implications for nanoelectronic and electromechanical devices.

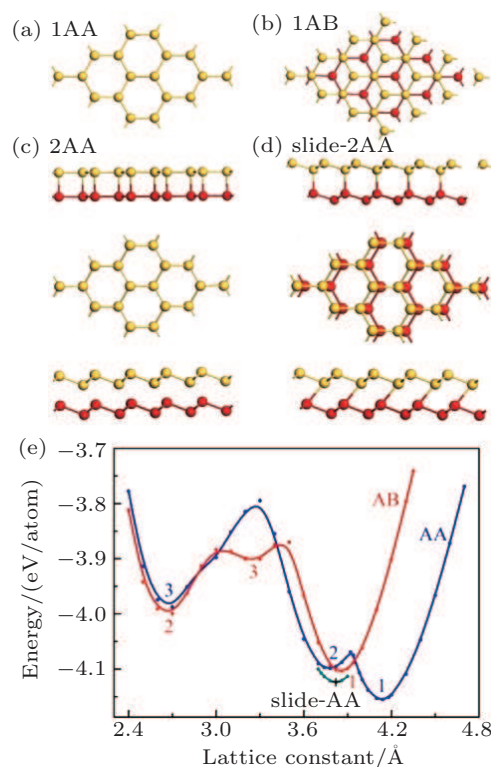


Fig. 2. Upper panels: Top and side views of (a) 1AA, (b) 1AB, (c) 2AA, and (d) slide-2AA structures of BLS. Lower panel (e): Cohesive energy (PBE level) versus lattice constant for AA (blue line) and AB (red line) stacking modes. The labels 1, 2, 3 in blue and red fonts denote each of three minima found for AA and AB modes, respectively. The cohesive energy of slide-2AA versus lattice constant (cyan short curve) is also shown.^[7]

3. Structures of silicene on Ag (111)

3.1. Single layer silicene on Ag (111)

As the sp^2 -hybridized Si is not stable in nature, the only way to synthesize silicene is to grow it on substrates in vacuum. Growth of SLS on Ag (111) by MBE was first reported by Aufray *et al.* in 2010.^[44] However, the results claimed in this work are seriously doubted, since the measured lattice constant of the honeycomb structure in their STM image is 17% shorter than the predicted lattice constant of free-standing silicene. In the same year, fabrication of silicene nanoribbons on Ag (110) surface was also reported by Le Lay *et al.*^[23] People usually choose silver as the supporting substrate for silicene because silver cannot form an alloy with silicon.

In 2012, the dynamics for growth of SLS on Ag (111) were convincingly studied independently by both Wu *et al.*^[10] and Le Lay *et al.*^[14] The experiments were performed in an ultra-high-vacuum (UHV) chamber combined with a homemade low-temperature STM. Silicon was evaporated from a heated Si wafer with a deposition flux onto a single-crystal Ag (111) substrate. The STM observations were performed at liquid nitrogen temperature (77 K) and liquid helium temperature (4 K) with chemically etched tungsten tips. All the STM data were recorded in the constant-current mode. The differential conductance (dI/dV) maps were extracted from

the lock-in signal by applying a modulation of 20 mV at 777 Hz to the tip bias. By carefully changing the temperature of substrate and the amount of deposited Si atoms, the phase diagram of silicene growth on Ag (111) was obtained. As shown in Fig. 3(d), the Si atoms form clusters below 400 K, and form several metastable reconstructed surfaces strongly bonded to the substrate: in the range from 400 K to 530 K, the $\sqrt{13} \times \sqrt{13}$ reconstruction (Fig. 3(a)) appeared on the Ag (111); 4×4 reconstruction (Fig. 3(b)) appeared from 400 K to 470 K; and $\sqrt{7} \times \sqrt{7}$ reconstruction (Fig. 3(c)) appeared from 470 K to 530 K. Then, $\sqrt{3} \times \sqrt{3}$ SLS with respect to Si (111)- 1×1 formed in a very narrow temperature window higher than 530 K.

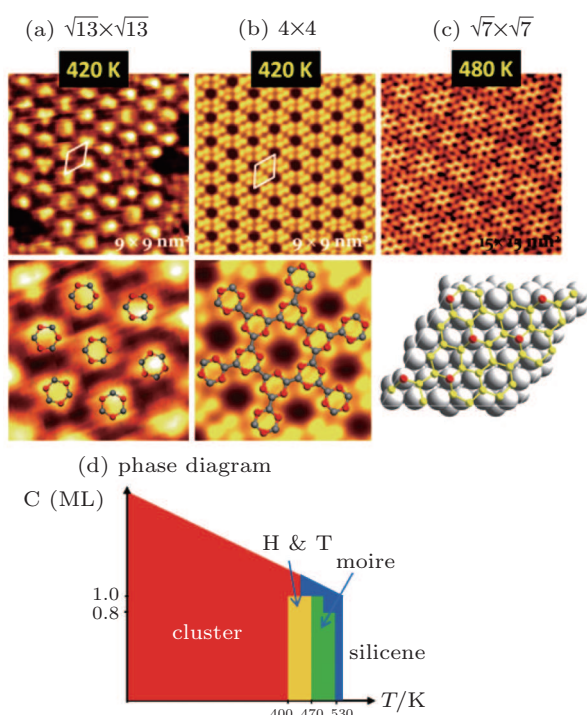


Fig. 3. Large scale (upper panels) and high resolution (lower panels) STM images of (a) $\sqrt{13} \times \sqrt{13}$, (b) 4×4 , and (c) $\sqrt{7} \times \sqrt{7}$ silicene superlattices with respect to Ag (111). Red balls in the lower panels denote highly buckled Si atoms. (d) Phase diagram of SLS growth on Ag (111).^[10]

Unlike the metastable silicon layer mentioned before, in which silicon atoms are strongly bonded to silver, the SLS formed at high temperature has very different structural properties,^[9] such as a constant height of 0.26 nm and a linear dispersive surface state, which will be discussed in the following sections. As shown in Fig. 4(a), large scale SLS films were obtained, which exhibit perfect layered structure and continuously cover the different height stages of the substrate. A high resolution STM image shows that this silicon film has the same honeycomb structure (Fig. 4(b)) as DFT-predicted silicene; however, its lattice constant (0.67 nm) is $\sqrt{3}$ times that of free-standing silicene (0.387 nm), leading to a $\sqrt{3} \times \sqrt{3}$ structure reconstruction. This structure is also confirmed by the low-energy electron diffraction (LEED) pattern (Fig. 4(c)). Other interesting phenomena were found for

$\sqrt{3} \times \sqrt{3}$ silicene. For example, the honeycomb $\sqrt{3} \times \sqrt{3}$ silicene undergoes a symmetry-broken phase transition to rhombic lattice below 40 K.^[18] The exploration of $\sqrt{3} \times \sqrt{3}$ silicene on Ag (111) requires a reasonable atomic model that is very different from the free-standing silicene model.

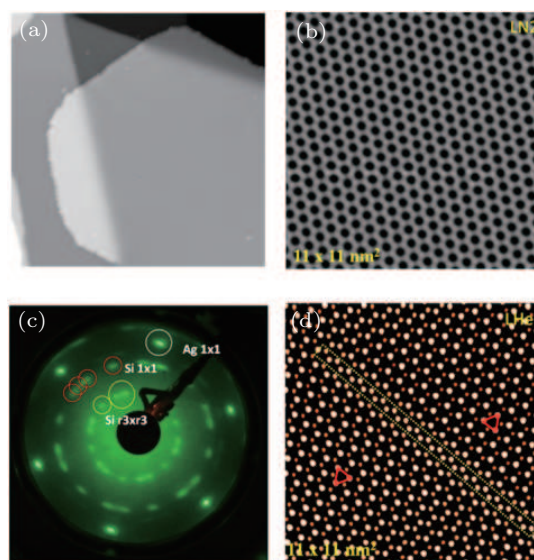


Fig. 4. (a) Large scale and (b) high resolution STM images of $\sqrt{3} \times \sqrt{3}$ silicene at tip bias 1.0 V at 77 K. (c) LEED pattern of $\sqrt{3} \times \sqrt{3}$ silicene at 51.4 eV. (d) Filtered high resolution STM images of $\sqrt{3} \times \sqrt{3}$ silicene at 0.1 V at 4 K.^[18]

In order to understand the observed $\sqrt{3} \times \sqrt{3}$ lattice constant of silicene on Ag (111) and the phase transition at low temperature, first-principles calculations were carried out to study SLS on Ag (111).^[18] The dispersion-corrected vdW-DFT^[45] was employed for structural research of the silicon monolayer adsorbed on Ag (111). The PAW pseudopotentials combined with a plane-wave basis set (energy cutoff at 250 eV) were used with Vienna *ab initio* Simulation Package (VASP).

After trying various prototype supercells to model epitaxial silicene, a reasonable atomic model of $\sqrt{3} \times \sqrt{3}$ silicene was proposed. As shown in Figs. 5(a) and 5(c), a rhombic $\sqrt{3} \times \sqrt{3}$ silicene layer on Ag (111) was relaxed from the DFT calculation, which is consistent with the STM investigation of $\sqrt{3} \times \sqrt{3}$ silicene in liquid helium (Fig. 4(d)). In this rhombic $\sqrt{3} \times \sqrt{3}$ silicene layer, the positions of a small proportion of the silicon atoms stand out from the silicene layer prominently, with the buckling distance of ~ 1.2 Å (red balls in Fig. 5), and the remaining silicon atoms are at an almost consistent height (yellow balls in Fig. 5), much lower and much more strongly bonded to the substrate. The energy-degenerated mirror-symmetrical structure of the rhombic $\sqrt{3} \times \sqrt{3}$ silicene was also found, as shown in Figs. 5(b) and 5(d). The consequent question is why does the $\sqrt{3} \times \sqrt{3}$ silicene look like a honeycomb structure at 77 K?

The scanned transition barrier for these two mirror-symmetrical $\sqrt{3} \times \sqrt{3}$ silicene isomers is low (~ 35 meV),

as demonstrated in Fig. 5(f)), indicating that the two configurations can freely transform to each other at high temperature. Because the scanning rate of the STM tip is much lower than the rapid transitions between these two energy minima, in the STM image at 77 K, we can observe only the superposition of them, appearing as a honeycomb structure, as displayed in Fig. 5(e). Therefore, the dynamical transition model can perfectly explain the symmetry-broken phase transition of $\sqrt{3} \times \sqrt{3}$ silicene at low temperature.

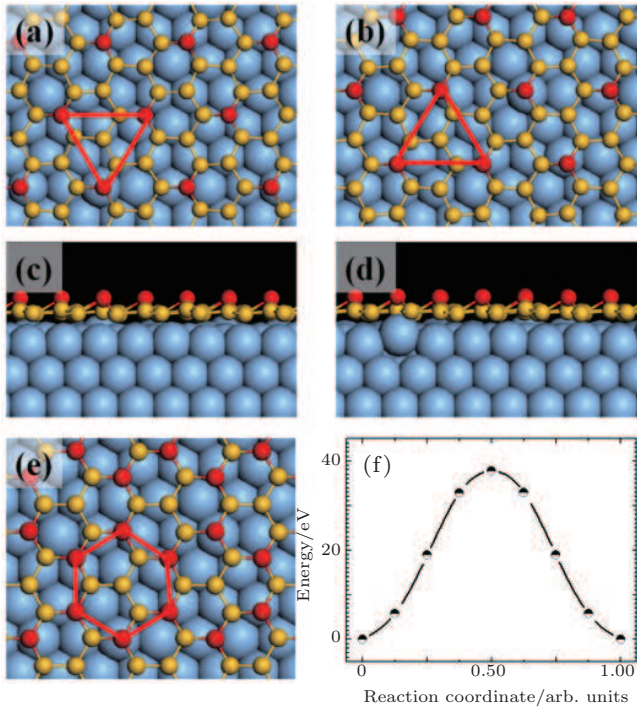


Fig. 5. Top views [(a) and (b)] and side views [(c) and (d)] of two mirror-symmetrical $\sqrt{3} \times \sqrt{3}$ silicene sheets on Ag (111) surface, obtained from DFT optimization in the case of lattices of both $\sqrt{3}$ silicene and silver substrate having identical directions. (e) Top views of superposition of structures in panels (a) and (b). Color code: Blue large balls, yellow small balls, and red small balls denote Ag atoms, Si atoms in the lower layer, and Si atoms in the higher layer, respectively. The red triangles denote the units of $\sqrt{3}$ silicene in (a) and (b) structures. (f) Scanned transition barrier between two symmetrical $\sqrt{3} \times \sqrt{3}$ counterparts.^[18]

3.2. The electronic structure of SLS on Ag (111)

The most attractive property of silicene is its novel electronic properties, especially its potential to support linear dispersive Dirac fermions like those of graphene.^[2] In addition, measuring the characteristic electronic structure of SLS provides further proof of the proposed silicene model on Ag (111). Thus, the electronic structure of SLS on Ag (111) has been intensively studied by both experiments and calculations. However, there are still debates on whether SLS can sustain electronic properties comparable to those of free-standing silicene, due to the Si–Ag interaction.^[11,46–48]

One way to probe the Dirac-type electrons is to investigate the quasiparticle interference (QPI) pattern based on STS.^[18,21] For example, the constant energy contours (CECs) in reciprocal space around the Dirac cone form small circles

centered at the high symmetry K points; therefore, free carriers are scattered both within the small circles (intravalley scattering) and between circles (intervalley scattering), resulting in unique QPI patterns in real space. Similar QPI patterns have been observed for $\sqrt{3} \times \sqrt{3}$ SLS on Ag (111). It should be noted the Dirac cone in $\sqrt{3} \times \sqrt{3}$ SLS should be located in the high symmetry Γ point, due to the $\sqrt{3}$ superlattice. In experiment, some multilayer islands have been found on the SLS, as shown in Fig. 6(a). Wavelike QPI patterns of the dI/dV map (Fig. 6(b)) near the edge of the island can be clearly seen. By analyzing the QPI patterns at different energy ranges near the Fermi level, the quasiparticle energy–momentum dispersion relation was drawn, as shown in Fig. 6(c), displaying a clear linear plot. Such a linear relation can also be reflected by the decay rate of the dI/dV intensity with increasing distance from the step edge of a bilayer silicene island, as in the example shown in Fig. 6(d). The oscillatory decaying intensity can be fitted using the equation for Friedel oscillations, $\delta\rho(x) \propto \cos(2kx + \phi)x^\alpha$, in which k is the wave vector of a standing wave and α is the decay factor. It is fitted as $\alpha = -1.5$ for an armchair edge (Γ – K direction) and $\alpha = -1.0$ for a zigzag edge (Γ – M direction). Such a fast decay rate is a characteristic of Dirac-type electrons, also reported for graphene^[49] and 3D topological insulators.^[50,51] On the other hand, a much slower decay rate ($\alpha = -0.5$) is observed for ordinary 2D electron gas (2DEG) systems, such as Cu (111).^[52]

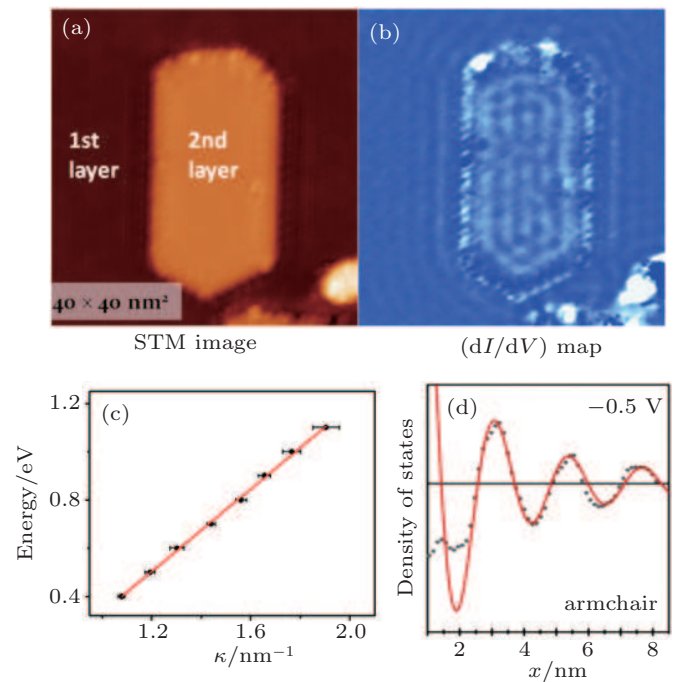


Fig. 6. (a) STM image (40 nm \times 40 nm) of SLS surface containing an island of BLS, taken at tip bias -1.0 V. (b) dI/dV map of the same area as panel (a), taken at tip bias of 0.5 V. (c) Energy dispersion as a function of κ for silicene, determined from the wavelength of QPI patterns. (d) LDOS on SLS as a function of distance from armchair edges at -0.5 V. The position of step edge is set at $x = 0$. Gray dots, experimental values; red lines, fits to the data.^[9,21]

The Dirac cone in the band structure of distorted $\sqrt{3} \times \sqrt{3}$ silicene is also confirmed by first principles calculations.^[18,21] As shown in Fig. 7(a), the band structure of isolated $\sqrt{3} \times \sqrt{3}$ distorted silicene is similar to that of 1×1 silicene (Fig. 7(b)). However, there is a small band gap (~ 0.15 eV) at the Dirac cone, and a flat band within the gap is contributed by the high-buckled Si atoms. Another interesting characteristic for electronic structure of $\sqrt{3} \times \sqrt{3}$ silicene is that its Dirac cone is located at the Γ point, which has six-fold symmetry, instead of the Dirac cone for graphene, located at the three-fold symmetric K point. As a result, at the high energy region of the Dirac cone for $\sqrt{3} \times \sqrt{3}$ silicene, we should observe hexagonal energy warping. Such hexagonal warping is confirmed by both DFT calculation (Fig. 7(c)) and fast Fourier transform of the dI/dV map. The linear dispersive bands of SLS on Ag (111) were also observed by ARPES measurement.^[14]

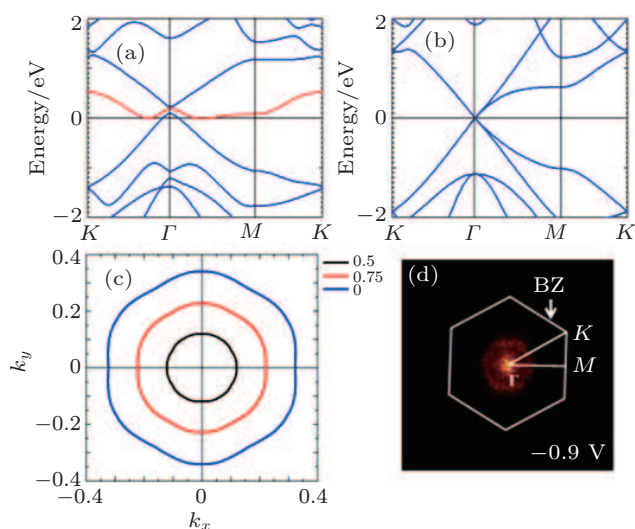


Fig. 7. (a) and (b) Band structures of the $\sqrt{3} \times \sqrt{3}$ structure of silicene layer and 1×1 structure of free-standing silicene, respectively. (c) Constant energy contours of the Dirac cone of $\sqrt{3} \times \sqrt{3}$ SLS from DFT calculations. (d) A k -space map obtained by Fourier transform of the dI/dV map at voltages of -0.9 V. The hexagon of 1×1 BZ is superimposed.^[18,21]

3.3. SLS on other substrates

SLS has also been grown on substrates other than silver. For example, experimental evidence for epitaxial SLS on ZrB_2 (0001) thin film and the Ir (111) surface was reported by Yamada-Takamura *et al.*,^[11] and Gao *et al.*,^[12] respectively. It is interesting that SLS films on both these substrates also adopt $\sqrt{3} \times \sqrt{3}$ reconstructions similar to those on Ag (111), as displayed by the DFT optimized structures in Figs. 8(a) and 8(b). Similar $\sqrt{3} \times \sqrt{3}$ SLS structures on Ag (111), ZrB_2 (0001), and Ir (111), which have different lattice constants, indicate the $\sqrt{3} \times \sqrt{3}$ superstructure should be a universal configuration of silicene on substrates, perhaps because the highly buckled Si atoms are closer to pure sp^3 -hybrid, and the lower Si atoms are more strongly bonded to the substrate. The first-principles calculations reveal the SLS–substrate interactions

are much stronger on ZrB_2 and Ir (111), implying electronic properties of SLS on either of these substrates should be much different from those of free-standing silicene.

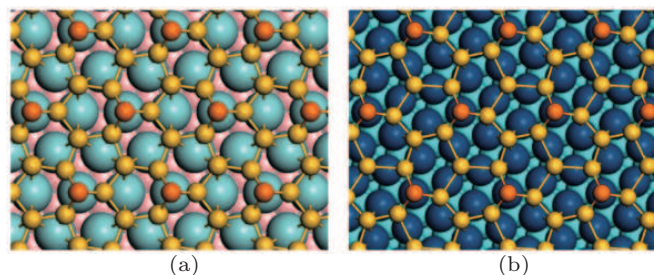


Fig. 8. Top views of $\sqrt{3} \times \sqrt{3}$ SLS films on (a) ZrB_2 (0001) and (b) Ir (111), obtained from DFT structural optimization. The orange balls denote highly buckled Si atoms.^[11,12]

4. Multilayer silicene (MLS) on Ag (111)

Beyond SLS, MLS has also been studied on Ag (111).^[22,24–29] As shown in Fig. 6(a), the multilayer silicene islands always exist on synthesized SLS. Recent experiments show MLS on Ag (111) can grow in a layer-by-layer fashion up to ~ 50 layers (L) or more.^[22] Unlike various metastable morphologies of SLS on Ag (111), MLS always assumes a unique $\sqrt{3} \times \sqrt{3}$ structure. Padova *et al.* proposed that Si layers in MLS are van der Waals packed, as evidenced by height measurements of Si layers and vibration spectra;^[27] on the other hand, Mannix *et al.* proposed that MLS has a structure identical to that of bulk silicon.^[28] Shirai *et al.* proposed that $\sqrt{3}$ reconstruction might be determined by the Ag atoms on the Si (111) surface.^[29] To better understand the structure and properties of MLS, we and our collaborators also did comprehensive experiments and calculations on MLS/Ag (111) systems.^[22]

The experimental method for studying MLS was the same as in the SLS study. Consistent with other reports, our STM images show that MLS samples always adopt a $\sqrt{3} \times \sqrt{3}$ super lattice, from monolayer to ~ 50 layers. The stacking mode of MLS can be determined by STM images of coexisting 1–3 layers of silicene, as shown in Figs. 9(a)–9(c). By aligning the lattices of 3 silicene layers, it can be confirmed that MLS is ABC-stacked, the same as bulk silicon. The height measurement (Fig. 9(d)) shows the interlayer distance is constant (~ 3.1 Å) with varying thickness of MLS. Thus, the STM investigation indicates MLS may have a diamond-like stacking style, as does bulk silicon.

Similar to our STS analysis of SLS, we probed the electronic structure of MLS using QPI. The standing wave can be seen in the typical dI/dV map of MLS shown in Fig. 9(e). It is interesting that a linear quasiparticle energy–momentum dispersion relation is obtained from the dI/dV maps at various energy ranges, as shown in Fig. 9(f), indicating that MLS has linear dispersive bands similar to those of SLS. This result

contradicts our previous findings that the Dirac-type electrons exist only for free-standing monolayer silicene.

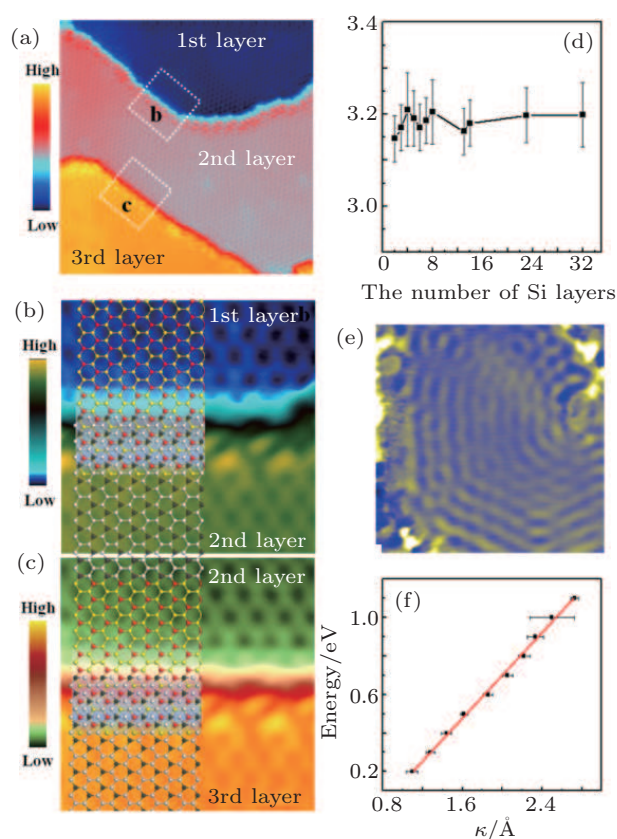


Fig. 9. (a) STM image ($V_{\text{tip}} = 1.2$ V) of coexisting SLS, BLS, and trilayer silicene films. (b) and (c) High resolution STM images of area labeled by white squares in panel (a). The atomic structure of the $\sqrt{3} \times \sqrt{3}$ silicene is superimposed, indicated that the stacking sequence of the adjacent Si layers is ABC stacking. (d) Measured height of topmost single atomic slice of MLS/Ag (111). (e) dI/dV map ($V_{\text{tip}} = -0.4$ V) on the surface of MLS/Ag (111) with obvious standing waves of surface states. (f) Linear energy-momentum dispersion by measuring the wavelength of standing waves in dI/dV maps under different bias.

To understand the experimentally observed $\sqrt{3} \times \sqrt{3}$ MLS morphology, as well as the unusual linear dispersive bands, we employed first-principles calculations to illustrate the structural origin and electronic nature of MLS. We deposited free-standing single-layer silicon onto Si/Ag (111) in a layer-by-layer fashion and relaxed the structure to mimic the growth mode of MLS in MBE experiments, and the initial structure was set to either AA or AB stacking.

In the calculation, the MLS is initially van der Waals packed, but during the optimization process it spontaneously forms interlayer covalent bonds leading to a diamond bulk structure; at the same time, a $\sqrt{3} \times \sqrt{3}$ surface relaxation similar to that in SLS also occurs, consistent with the STM observation. The side view of calculated 5-layer MLS is exhibited in Fig. 10(a). One possible reason for the spontaneous formation of covalent bonds is that a highly buckled Si atom in epitaxial silicene has one dangling bond, making the silicene surface more reactive. Considering this along with STM ob-

servations and first principles calculations, it can be concluded $\sqrt{3} \times \sqrt{3}$ surface relaxation is a universal feature for MLS on Ag (111).

It is interesting that the $\sqrt{3} \times \sqrt{3}$ superstructure automatically form on both surfaces, after we peeling off the Ag (111) substrate from the MLS, as shown in Fig. 10(b). Therefore, the $\sqrt{3} \times \sqrt{3}$ superstructure exists for both epitaxial and free-standing MLS, indicating that this is a universal surface feature for Si thin films, irrelevant to substrate effects. In the literature, it is reported that Ag and Si atoms have close electronegativities; in addition, the MLS and SLS on Ag (111) have very close cohesive energies, implying that SLS on Ag (111) has properties similar to those of MLS. As a result, the $\sqrt{3} \times \sqrt{3}$ surface relaxation is universal for Si thin films and SLS on Ag (111).

We further calculate the band structure respectively projected to MLS and Ag (111) for MLS/Ag (111). As shown in Fig. 10(c), a cone-like surface state is found near the Fermi level for MLS. Such a cone-like surface state can provide MLS the signature Dirac-type electrons, which can be observed by both STS and ARPES. The Fermi velocity obtained from the slope of this surface state is in close agreement with the previous ARPES measurement.^[24] Analysis shows that most Si atoms in flat-lying positions have formed delocalized π bonds leading to a Dirac band structure. It should be mentioned that another cross of linear bands is also clearly observed for Ag (111) substrate (Fig. 10(d)), which is the effect of band folding of bulk Ag (111) in the Brillouin zone of the $\sqrt{3} \times \sqrt{3}$ superlattice of silicene and is irrelevant to the electronic structure of silicene.

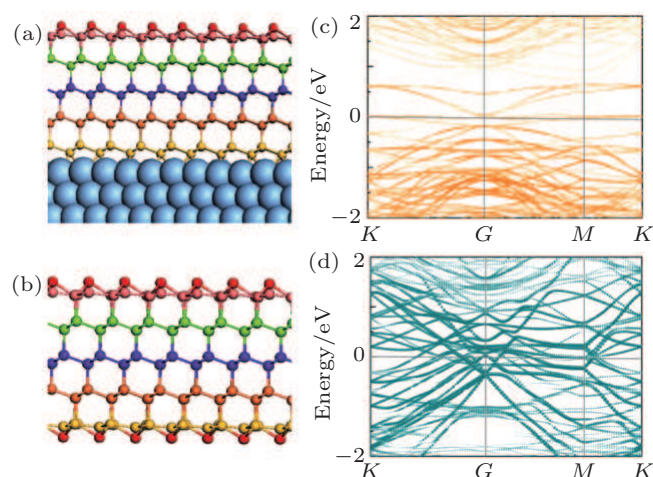


Fig. 10. (a) Side view of 5-layer MSL on Ag (111) based on DFT calculation. (b) Side view of free-standing 5-layer MSL thin film. The electronic band structure is projected onto (c) MLS and (d) Ag (111) substrates, respectively. The size of dots corresponds to the weight of the contribution.

It is known that conventional bulk Si (111) surfaces obtained from traditional treatments always forms drastic reconstructions, including 2×1 , 5×5 , and the complicated dimer-adatom-stacking fault (DAS) configuration of Si (111)- 7×7 .

These reconstructions are accompanied by serious bond breaking/reforming to saturate dangling bonds.^[53–59] On the other hand, the morphology of MLS grown at much lower temperatures represents a new bottom-up approach to obtaining an ideal Si (111)- 1×1 surface that preserves the original hexagonal bond topology and holds a Dirac-type surface state. In addition, recent work has found that MLS is robust in air,^[26] which greatly increases the potential for its practical application. The study of MLS provides new fundamental understanding of silicon and encourages hope for the future development of Si-compatible devices.

5. Hydrogenation of silicene

Due to the potential application of graphene as hydrogen storage material, and a requirement of modification for obtaining the zero-gap electronic structure, hydrogenation of graphene has been widely studied in recent years.^[60] As mentioned before, Si atoms in silicene are partially sp^3 -hybridized, giving silicene stronger reactivity than pure sp^2 -hybridized graphene. As a result, silicene should be easier to hydrogenate. Pioneering theoretical work on freestanding H-doped silicene showed that hydrogenation can bring significant modifications to silicene, such as large band gap,^[30] ferromagnetism,^[32] and optoelectronic properties.^[33] Recently, with our collaborators, we did the first-ever STM experiment combined with first principles calculations on the hydrogenation of SLS on Ag (111).^[34]

The experiments were based on the 3×3 SLS (with respect to the Si (111)- 1×1 lattice) on Ag (111) grown using the method mentioned before, as this silicene phase is the simplest and most well understood. The SLS surface at room temperature was then exposed to dissociated H_2 gas from a hot tungsten filament. The calculation details are also the same as the computational method described before.

High resolution STM images reveal that the hydrogenated 3×3 SLS/Ag (111) has two kinds of hydrogenation pattern: 7H-adsorption and 6H-adsorption, as respectively shown in Figs. 11(a) and 11(b), indicating that the SLS is not fully hydrogenation-saturated. The coexistence of different hydrogenation patterns can be found in Fig. 11(b). This phenomenon can be explained by the lateral shift of SLS or the change of buckling Si atoms after hydrogenation. The first-principles calculations give the exact models for both hydrogenation patterns, as respectively illustrated in Figs. 11(c) and 11(d). The simulated STM images for both hydrogen adsorption modes (Figs. 11(e) and 11(f)) closely agree with the experimental STM images. Coverage in Fig. 11(d) is higher than in Fig. 11(c), implying that hydrogenated silicene prefers to adopt the latter structure in a hydrogen atmosphere. This is consistent with the experimental observation that most hydrogenation patterns are the same as that in Fig. 11(a). The bind-

ing energy of H atoms for the two configurations also shows that the hydrogenated 3×3 SLS with 7H atoms in one unit cell is more stable. It is noted that the predicted band gap of free-standing H-silicene was not observed, due to the Si–Ag interaction.

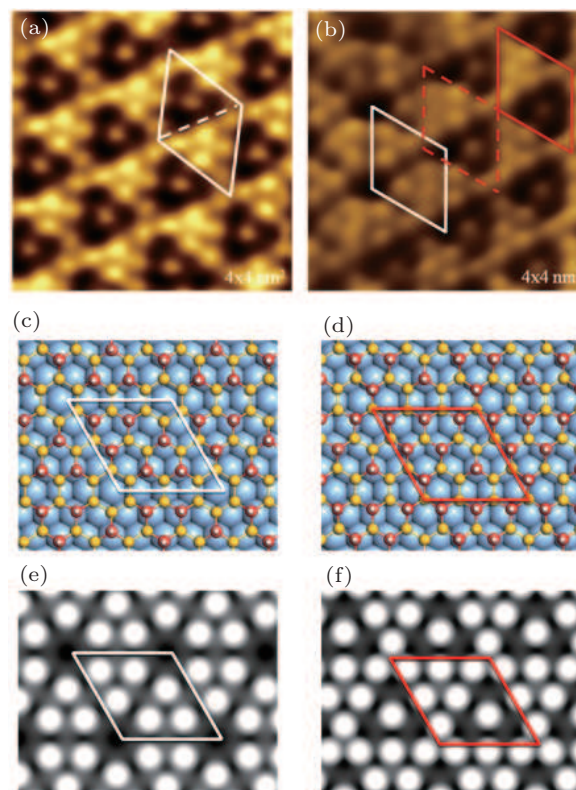


Fig. 11. (a) STM image of 7H-hydrogenated 3×3 SLS/Ag (111). The white rhombus marks a unit cell of the structure. (b) Coexistence of 7H-hydrogenated (red cell) and 6H-hydrogenated (white cell) SLS. The structural models of (c) 6H-hydrogenated and (d) 7H-hydrogenated SLS from DFT optimizations; corresponding simulated STM images are shown in panels (e) and (f), respectively.^[34]

Another important feature of hydrogenated 3×3 SLS is reversible dehydrogenation. Fully hydrogenated SLS can be completely restored to its original state by increasing the temperature to ~ 450 K. Such easily reversible hydrogenation suggests that silicene could be used for hydrogen storage. Our work on silicene hydrogenation has pioneered the area, enabling further investigation of the electronic properties of hydrogenated silicene.

6. Conclusion and outlook

In this review, we have summarized some experiment and theoretical studies of silicene, mainly work done by us and our collaborators since 2012. We introduced three areas of silicene research: pure theoretical prediction of configurations and electronic properties of SLS and BLS, combined experimental-theoretical studies of SLS and MLS, and hydrogenated SLS on Ag (111) substrate. Free-standing silicene is theoretically predicted to have a simple 2D honey-

comb structure and signature Dirac bands. However, according to the work reviewed here, it is found that SLS on Ag (111) is an extremely complex system. For MLS, the stacking style of silicene layers makes the system even more complicated. Thus, to figure out the atomic and electronic structure of silicene/Ag (111) is much more difficult than we expected when we started looking into the subject. Even though the highest resolution STM observation and extensive first principles calculations were employed, we can only propose some reasonable models and explanations of such systems. So nowadays, the structure and electronic properties of silicene on Ag (111) are still under debate.

Our studies demonstrate that, among all the metastable phases of SLS on Ag (111), the $\sqrt{3} \times \sqrt{3}$ phase has the weakest interaction with the substrate and preserves the Dirac-type band structure of silicene. Although the calculations show that different stacking modes can induce various metastable silicene configurations such as various bilayer silicene morphologies, MLS on Ag (111) adopts only diamond-like stacking like that of bulk silicon, as well as a unique $\sqrt{3} \times \sqrt{3}$ surface relaxation, similar to the $\sqrt{3} \times \sqrt{3}$ phase of SLS. It is remarkable that MLS on Ag (111) still has a surface state with linear-dispersive bands, indicating great potential for electronic devices based on MLS. In addition, we did pioneering research on hydrogenation of silicene. It was found that silicene is easier to hydrogenate than graphene, and a reversible hydrogenation phenomenon was found, indicating silicene may be a promising material for hydrogen storage.

Finally, although silicene systems have been intensively studied during these years, this is still just the beginning of silicene research. As we mentioned, the model of silicene on Ag (111) is still under debate. The main reason is that Si–Ag interaction is quite strong, which may seriously interfere with the electronic properties of silicene adsorbed on it. Furthermore, because the metallic properties of Ag can overwhelm the electronic properties of silicene, it is difficult to distinguish information about electrons of silicene from that about substrate electrons. Therefore, to grow silicene on a weakly interacting semiconductor substrate is the most urgent task for future study of silicene. In addition, since silicene is easier to functionalize than graphene, using different elements to dope silicene can be another important subject in the coming years.

References

- [1] Geim A K and Novoselov K S 2007 *Nat. Mater.* **6** 183
- [2] Cahangirov S, Topsakal M, Aktürk E, Sahin H and Ciraci S 2009 *Phys. Rev. Lett.* **102** 236804
- [3] Liu C C, Feng W and Yao Y G 2011 *Phys. Rev. Lett.* **107** 076802
- [4] Ezawa M 2012 *New J. Phys.* **14** 033003
- [5] Liu F L, Liu C C, Wu K H, Yang F and Yao Y G 2013 *Phys. Rev. Lett.* **111** 066804
- [6] Pan H, Li Z, Liu C C, Zhu G, Qiao Z and Yao Y G 2014 *Phys. Rev. Lett.* **112** 106802
- [7] Fu H X, Zhang J, Ding Z J, Li H and Meng S 2014 *Appl. Phys. Lett.* **104** 131904
- [8] Bai J, Tanaka H and Zeng X C 2010 *Nano Research* **3** 694
- [9] Chen L, Liu C C, Feng B, He X, Cheng P, Ding Z, Meng S, Yao Y G and Wu K H 2012 *Phys. Rev. Lett.* **109** 056804
- [10] Feng B, Ding Z J, Meng S, Yao Y G, He X Y, Cheng P, Chen L and Wu K H 2012 *Nano Lett.* **12** 3507
- [11] Fleurence A, Friedlein R, Ozaki T, Kawai H, Wang Y and Yamada-Takamura Y 2012 *Phys. Rev. Lett.* **108** 245501
- [12] Meng L, Wang L, Zhang L, Du S, Wu R, Li L, Zhang Y, Li G, Zhou H, Hofer W A and Gao H J 2013 *Nano Lett.* **13** 685
- [13] Chiappe D, Scalise E, Cinquanta E, Grazianetti C, Broek B, Fanciulli M, Houssa M and Molle A 2014 *Adv. Mater.* **26** 2096
- [14] Vogt P, De Padova P, Quaresima C, Avila J, Frantzeskakis E, Asensio M C, Resta A, Ealet B and Le Lay G 2012 *Phys. Rev. Lett.* **108** 155501
- [15] Lin C L, Arafune R, Kawahara K, Tsukahara N, Minamitani E, Kim Y, Takagi N and Kawai M 2012 *Appl. Phys. Express* **5** 045802
- [16] Jamgotchian H, Colington Y, Hamzaoui N, Ealet B, Hoarau J, Aufray B and Biberian J P 2012 *J. Phys.: Condens. Matter* **24** 172001
- [17] Chiappe D, Grazianetti C, Tallarida G, Fanciulli M and Molle A 2012 *Adv. Mater.* **24** 5088
- [18] Chen L, Li H, Feng B, Ding Z, Qiu J, Cheng P, Wu K H and Meng S 2013 *Phys. Rev. Lett.* **110** 085504
- [19] Chen L, Liu C C, Feng B, He X, Cheng P, Ding Z, Meng S, Yao Y and Wu K H 2013 *Phys. Rev. Lett.* **110** 229702
- [20] Chen L, Feng B and Wu K H 2013 *Appl. Phys. Lett.* **102** 081602
- [21] Feng B, Li H, Liu C C, Shao T, Cheng P, Yao Y, Meng S, Chen L and Wu K H 2013 *ACS Nano* **7** 9049
- [22] Chen J, Li W, Feng B, Cheng P, Qiu J, Chen L and Wu K arXiv: 1405.7534
- [23] Aufray B, Kara A, Vizzini S, Oughaddou H, Léandri C, Ealet B and Le Lay G 2010 *Appl. Phys. Lett.* **96** 183102
- [24] Padova P D, Avila J, Resta A, Colambo I R, Quaresima C, Ottaviani C, Olivieri B, Bruhn T, Vogt P, Asensio M C and Le Lay G 2013 *J. Phys.: Condens. Matter* **25** 382202
- [25] Vogt P, Capiod P, Berthe M, Resta A, De Padova P, Bruhn T, Le Lay G and Grandidier B 2014 *Appl. Phys. Lett.* **104** 021602
- [26] Padova P D, Ottaviani C, Quaresima C, Olivieri B, Imperatori P, Salomon E, Angot T, Quagliano L, Romano C, Vona A, Muniz-Miranda M, Generosi A, Paci B and Le Lay G 2014 *2D Materials* **1** 021003
- [27] Padova P D, Vogt P, Resta A, Avila J, Colambo I R, Quaresima C, Ottaviani C, Olivieri B, Bruhn T, Hirahara T, Shirai T, Hasegawa S, Asensio M C and Le Lay G 2013 *Appl. Phys. Lett.* **102** 163106
- [28] Mannix A J, Kiraly B, Fisher B L, Hersam M C and Guisinger N P 2014 *ACS Nano* **8** 7538
- [29] Shirai T, Shirasawa T, Hirahara T, Fukui N, Takahashi T and Hasegawa S 2014 *Phys. Rev. B* **89** 241403
- [30] Lew Yan Voon L C, Sandberg E, Aga R S and Farajian A A 2010 *Appl. Phys. Lett.* **97** 163114
- [31] Houssa M, Scalise E, Sankaran K, Pourtois G, Afanas'ev V V and Stesmans A 2011 *Appl. Phys. Lett.* **98** 223107
- [32] Zheng F B and Zhang C W 2012 *Nano. Res. Lett.* **7** 422
- [33] Huang B, Deng H X, Lee H, Yoon M, Sumpter B G, Liu F, Smith S C and Wei S H 2014 *Phys. Rev. X* **4** 021029
- [34] Qiu J, Fu H, Shao T, Xu Y, Li H, Meng S, Chen L and Wu K 2015 *Phys. Rev. Lett.* **114** 126101
- [35] Morishita T, Nishio K and Mikami M 2008 *Phys. Rev. B* **77** 081401R
- [36] De Padova P, Kubo O, Olivieri B, Quaresima C, Nakayama T, Aono M and Le Lay G 2012 *Nano Lett.* **12** 5500
- [37] Morishita T, Spencer M J S, Russo S P, Snook I K and Mikami M 2011 *Chem. Phys. Lett.* **506** 221
- [38] Luo W, Ma Y, Gong X and Xiang H 2014 *J. Am. Chem. Soc.* **136** 15992
- [39] Lian C and Ni J 2013 *AIP Adv.* **3** 52102
- [40] Perdew J P, Burke K and Ernzerhof M 1996 *Phys. Rev. Lett.* **77** 18
- [41] Heyd J, Scuseria G E and Ernzerhof M 2006 *J. Chem. Phys.* **124** 219906
- [42] Kresse G and Hafner J 1994 *J. Phys.: Condens. Matter* **6** 8245
- [43] Telling R H and Heggie M I 2003 *Phil. Mag. Lett.* **83** 411
- [44] Lalmi B, Oughaddou H, Enriquez H, Kara A, Vizzini S, Ealet B and Aufray B 2010 *Appl. Phys. Lett.* **97** 223109
- [45] Dion M, Rydberg H, Schroder E, Langreth D C and Lundqvist B I 2006 *Phys. Rev. Lett.* **92** 246401

- [46] Gori P, Pulci O, Ronci F, Colonna S and Bechstedt F 2013 *J. Appl. Phys.* **114** 113710
- [47] Tsoutsou D, Xenogiannopoulou E, Golias E, Tsipas P and Dimoulas A 2013 *Appl. Phys. Lett.* **103** 231604
- [48] Guo Z X and Oshiyama A 2014 *Phys. Rev. B* **89** 155418
- [49] Rutter G M, Crain J N, Guisinger N P, Li T, First P N and Stroscio J A 2007 *Science* **317** 219
- [50] Wang J, Li W, Cheng P, Song C, Zhang T, Deng P, Chen X, Ma X, He K and Jia J 2011 *Phys. Rev. B* **84** 235447
- [51] Alpichshev Z, Analytis J G, Chu J H, Fisher I R, Chen Y L, Shen Z X, Fang A and Kapitulnik A 2010 *Phys. Rev. Lett.* **104** 016401
- [52] Crommie M F, Lutz C P and Eigler D M 1993 *Nature* **363** 524
- [53] Schlier R E and Farnsworth H E 1959 *J. Chem. Phys.* **30** 917
- [54] Binning G, Rohrer H, Gerber C and Weibel E 1983 *Phys. Rev. Lett.* **50** 120
- [55] Bennett A, Feldman L C, Kuk Y, McRae E G and Rose J P 1983 *Phys. Rev. B* **28** 3656
- [56] McRae E G and Caldwell C W 1981 *Phys. Rev. Lett.* **46** 1632
- [57] McRae E G 1983 *Phys. Rev. B* **28** 2305
- [58] Takayanagi K, Tanishiro Y, Takahashi M and Takahashi S 1985 *J. Vac. Sci. Technol. A* **3** 1502
- [59] Takayanagi K, Tanishiro Y, Takahashi M and Takahashi S 1985 *Surf. Sci.* **164** 367
- [60] Balog R, Jørgensen B, Nilsson L, Andersen M, Rienks E, Bianchi M, Fanetti M, Lægsgaard E, Baraldi A, Lizzit S, Slijivancanin Z, Besenbacher F, Hammer B, Pedersen T G, Hofmann P and Hornekær L 2010 *Nat. Mater.* **9** 315